Land Subsidence Monitoring with Differential SAR Interferometry

Tazio Strozzi, Urs Wegmüller, Luigi Tosi, Gabriele Bitelli, and Volker Spreckels

Abstract

The potential of differential SAR interferometry for land subsidence monitoring is reported on. The principle of the technique and the approach to be used on a specific case are first presented. Then significant results using SAR data from the ERS satellites for various sites in Germany, Mexico, and Italy, representing fast (m/year) to slow (mm/year) deformation velocities, are discussed. The SAR interferometric displacement maps are validated with available leveling data. The accuracy of the subsidence maps produced, the huge SAR data archive starting in 1991, the expected continued availability of SAR data, and the maturity of the required processing techniques lead to the conclusion that differential SAR interferometry is suitable for operational monitoring of land subsidence.

Introduction

Land subsidence (land surface sinking) occurs in many parts of the world, particularly in densely populated regions on deltas (Poland, 1984; Barends *et al.*, 1995). Subsidence is the result of the natural compaction of sediments; of extraction of ground water, geothermal fluids, oil, gas, coal, and other solids through mining; and of underground construction. Most of the major subsidence areas around the world have developed in the past half-century at accelerated rates due to the rapidly increasing use of ground water, oil, and gas. Even if the hazards associated with subsidence are different from those caused by sudden and catastrophic natural events like floods and earthquakes, because surface sinking is a slow event, expansive damage can occur. In particular, many areas of known subsidence are along coasts where the phenomenon becomes obvious when the ocean or lake waters start coming further up on the shore. In addition, spatially heterogeneous subsidence produces damage in buildings and in other man-made structures such as bridges, highways, electric power lines, railroads, and underground pipes. Spatially heterogeneous subsidence is also the cause of changes in the drainage patterns, with canals that no longer carry their original design flows. For all these reasons, there is an increasing demand for accurate monitoring of land subsidence in order to improve the understanding of the phenomena and to give recommendations for a sustainable use of the underground resources.

T. Strozzi and Urs Wegmüller are with Gamma Remote Sensing, Thunstrasse 130, 3074 Muri BE, Switzerland (strozzi@gamma-rs.ch).

L. Tosi is with ISDGM, CNR, S. Polo 1364, 30124 Venezia, Italy.

G. Bitelli is with DISTART, University of Bologna, Viale Risorgimento 2, 40136 Bologna, Italy.

V. Spreckels is with the Institute for Photogrammetry and Engineering Surveys, University of Hannover, c/o Deutsche Steinkohle AG (DSK), DG, Gleiwitzer Platz 3, 46236 Bottrop, Germany.

The problems of land subsidence are a known environmental aspect in many cites and were among those included in the list of research projects recommended by UNESCO's International Hydrological Decade, which began in 1965, and the International Hydrological Program, a continuing UNESCO program beginning in 1975 (Barends *et al.*, 1995). Traditionally, land subsidence is determined with precision leveling surveys. Wide networks of benchmarks were set up in most of the subsiding cities, and measurements are periodically repeated (Figueroa Vega, 1976; Poland, 1984; Balestra and Villani, 1991; Brighenti, 1991; Capra *et al.*, 1991; Bertoni *et al.*, 1995; Carbognin *et al.*, 1995; Gottardi *et al.*, 1995). Leveling allows the monitoring of land subsidence in selected locations with high precision but is, for large areas, time consuming and expensive. Recently, GPS stations were implemented in few significant points of large subsiding areas in order to have a fast, cheap, and global measurement of subsidence (Bitelli *et al.*, 2000). In the context of traditional surveying techniques, differential SAR interferometry has the potential to provide very important subsidence information over urban areas because of its two-dimensional spatial coverage, its high vertical accuracy, the SAR data availability, and its competitive cost.

The potential of differential synthetic aperture radar (SAR) interferometry to map coherent displacements at centimeter to millimeter resolutions resulted in recent years in spectacular new results for the geophysical sciences. Earthquake displacement (Massonet *et al.*, 1993), volcano deformation (Massonet *et al.*, 1995), glacier dynamics (Goldstein *et al.*, 1993; Joughin, 1996, Mohr *et al.*, 1998), and land subsidence (Strozzi and Wegmüller, 1999; Strozzi *et al.*, 1999; Fruneau *et al.*, 1999; Ferretti *et al.*, 1999; Strozzi *et al.*, 2000b) were mapped. In the SAR interferometric approach, two SAR images are combined to exploit the phase difference of the signals. The interferometric phase is sensitive to both surface topography and coherent displacement along the look vector occurring between the acquisitions of the interferometric image pair. The basic idea of differential SAR interferometry is to subtract the topography related phase from the interferogram to derive a displacement map. For a specific case, different approaches can be applied depending on the availability of a digital elevation model (DEM), on the characteristics of the SAR data with respect to spatial baseline, on acquisition time difference and coherence, on the displacement rates and shapes, on the land cover, and on the topography. In this contribution we review the principles of the differential interferometric SAR technique for subsidence monitoring, discuss how the approach is adapted to a specific case, and present significant results for sites in Germany, Mexico, and

Photogrammetric Engineering & Remote Sensing
Vol. 67, No. 11, November 2001, pp. 1261–1270.

0099-1112/01/6711–1261$3.00/0

Italy. Because the results are based on SAR data from the European Remote Sensing Satellites ERS-1 and ERS-2, emphasis is given to the characteristics of these sensors. Taking into account the limitations of SAR interferometry in non-urban environments, we also propose a strategy for the integration of leveling, GPS, and SAR data in order to achieve an accurate, rational, and cost-effective monitoring.

Differential SAR Interferometry for Land Subsidence Monitoring

SAR Interferometry

In the interferometric approach, two SAR images acquired from slightly different orbit configurations and/or at different times are combined to exploit the phase difference of the signals (Zebker *et al.*, 1994; Bamler and Hartl, 1998; Wegmüller *et al.*, 1998; Mohr and Madsen, 1999). By assuming that the scattering phase is the same in both images, the interferometric phase ϕ is a very sensitive measure of the range difference $R_2 - R_1$: i.e.,

$$\phi = \phi_1 - \phi_2 = \frac{4\pi}{\lambda}(R_2 - R_1). \tag{1}$$

Here, ϕ_1 and ϕ_2 are the phases of the first and second SAR images, respectively; R_1 is the distance from the SAR to the scatterer by the first acquisition; R_2 is the distance by the second acquisition; and λ is the wavelength. The interferometric phase is determined as the argument of the normalized interferogram γ, defined as the normalized complex correlation coefficient of the complex electromagnetic fields s_1 and s_2 backscattered by the illuminated elements at positions R_1 and R_2: i.e.,

$$\gamma = \frac{\langle s_1 s_2^* \rangle}{\langle s_1 s_1^* \rangle \langle s_2 s_2^* \rangle}. \tag{2}$$

Here, the brackets $\langle s \rangle$ stand for the ensemble averaging of s, and s^* is the complex conjugate of s. Coherent averaging over statistically independent samples reduces the variance of the interferometric phase. The coherence $|\gamma|$, a measure of the phase noise, is the magnitude of the normalized interferogram. The coherence is limited to values in the interval from 0 to 1.

The interferometric phase is sensitive to both surface topography and coherent movement of the scatterer in the line-of-sight direction between the two observations, with inhomogeneous propagation delay (so-called atmospheric artifacts) and phase noise introducing the main error sources. For the purpose of this analysis, the interferometric phase is linearized as (Mohr and Madsen, 1999)

$$\phi = \frac{4\pi}{\lambda} B_{\parallel} + \frac{4\pi}{\lambda} r_{disp} + \frac{4\pi}{\lambda} r_{atmo} + \phi_{noise} \tag{3}$$

where $B_{\parallel}$ denotes the component of the baseline, i.e., of the separation of the two antennas in space, parallel with the line-of-sight direction, r_{disp} is the displacement of the scatterer in the line-of-sight direction, and r_{atmo} represents path length changes caused by different atmospheric conditions during the acquisitions of the two SAR images. The interferometric phase ϕ is still ambiguous to within integer multiples of 2π. The problem of overcoming this ambiguity through phase unwrapping is addressed in the next section.

Differentiation of the first term of Equation 3 with respect to the surface height yields the relationship between a change in the topographic height z and the corresponding change in the interferometric phase ϕ (Bamler and Hartl, 1998): i.e.,

$$\frac{\partial \phi}{\partial z} = \frac{4\pi}{\lambda} \frac{B_{\perp}}{R \sin\theta}. \tag{4}$$

Here, R is the distance from the SAR to the scatterer, θ is the incidence angle, and $B_{\perp}$ is the component of the baseline perpendicular to the line-of-sight direction. The baseline is small enough that R and θ can be assumed to be the same for both sensor positions. For the ERS SAR configurations, with a wavelength of 5.66 cm, a nominal incidence angle of 23°, and a nominal slant range of 853 km, Equation 4 reduces to

$$\frac{\partial \phi}{\partial z} = \frac{B_{\perp}[m]}{1500 m^2}. \tag{5}$$

For a perpendicular baseline component of 50 m, the topographic height change associated with a 2π cycle is 188 m. On the other hand, an error of 10 m in the estimation of the topographic height (e.g., as a consequence of an inaccurate DEM) results, for a perpendicular baseline component of 50 m, in a phase error of 0.11π. For interferograms with small perpendicular baseline components, the effect of the topographic related phase is very small but not negligible for extremely slow subsidence rates.

Differentiation of the first term of Equation 3 with respect to the slant-range distance y yields the fringe frequency in slant-range for a flat surface (Bamler and Hartl, 1998): i.e.,

$$\frac{\partial \phi}{\partial y} = \frac{4\pi}{\lambda} \frac{B_{\perp}}{R \tan\theta}. \tag{6}$$

Differentiation of the first term of Equation 3 with respect to the azimuth distance x yields the fringe frequency in azimuth for a flat surface

$$\frac{\partial \phi}{\partial x} = \frac{4\pi}{\lambda} \frac{\partial B_{\parallel}}{\partial x}. \tag{7}$$

Here, $\partial B_{\parallel}/\partial x$ represents the change of $B_{\parallel}$ along the line of flight as a result of non-parallel orbits.

The phase term related to the coherent displacement of the scattering center along the radar look vector, r_{disp}, may be transformed to a vertical displacement, r_{vert}, if deformation in vertical direction can be assumed: i.e.,

$$r_{vert} = \frac{r_{disp}}{\cos\theta}. \tag{8}$$

Here, coherent means that the same displacement of adjacent scatters is observed. In the case of ERS SAR data, a phase change of 2π corresponds to a vertical displacement of 3.07 cm. In general, however, surface deformations may also occur in directions other than the vertical. Strictly speaking, a single SAR interferometric observation does not allow the full determination of the magnitude and direction of a surface deformation, but allows only an observation of the deformation component along the radar look direction.

Changes in the effective path length between the SAR and the surface elements as a result of changing permittivity of the atmosphere lead to a non-zero atmospheric delay, r_{atmo}. The relevant changes in the atmospheric permittivity conditions are mainly associated with water vapor content. Heterogeneity of the water vapor content in the atmosphere can cause heterogeneity of the propagation delay. Currently, it does not seem to be possible to completely avoid these limitations. We address the minimization of errors introduced by atmospheric effects with the interferogram stacking technique (in a later section of this paper).

Finally, the standard deviation of the phase noise σ_{noise}, reached asymptotically for a large number of looks N, is a function of the coherence $|\gamma|$ (Rodriguez *et al.*, 1992): i.e.,

$$\sigma_{noise} = \frac{1}{2N} \frac{\sqrt{1 - |\gamma|^2}}{|\gamma|}. \quad (9)$$

The coherence can be divided into three dominant contributions (Bamler and Hartl): the influence of the signal-to-noise ratio $\gamma_{thermal}$, spatial decorrelation $\gamma_{spatial}$ related to the imaging geometry (interferometric baseline, local incidence angle), and temporal decorrelation $\gamma_{temporal}$. The thermal decorrelation is usually not a problem for the ERS SAR. Geometric decorrelation is related to the different look angles of the two SAR acquisitions and leads to a critical baseline over which the interferometric phase is pure noise. In the ERS case, the critical baseline for horizontal terrain is about 1150 m. The geometrical decorrelation effect related to surface scattering can be avoided using processing filters tuned to different center frequencies, a procedure known as spectral shift filtering, at the cost of a reduced range resolution (Gatelli *et al.*, 1994). However, effects of the terrain slope and of volume scattering are usually not considered in the spectral shift filtering and reduce the range of baselines useful for subsidence studies to values smaller than a few hundred of meters. Temporal decorrelation is the result of the changed geometrical configuration of the scatterers between the acquisitions of the interferometric pair (Strozzi *et al.*, 2000a). For example, water and forest show very low coherence even for acquisition time intervals of one day. Agricultural fields show intermediate coherence, still useful for phase interpretation after one or two months in temperate regions during the winter. Urban and arid areas, finally, show high coherence also for acquisition time intervals larger than one year. The main problems of high phase noise are the lack of spatial information for certain land-use classes and the difficulties in the phase unwrapping.

Differential SAR Interferometry

The basic idea of differential SAR interferometry is to separate the topography and displacement related phase terms to allow the mapping of displacement (Wegmüller *et al.*, 1998). In the so-called two-pass differential interferometry approach, the topography-related phase term is calculated from a DEM. Alternatively, in the so-called three-pass and four-pass approaches, the topographic-related phase term is estimated from an independent interferometric pair with a short acquisition time interval, such as an ERS-1/2 Tandem pair (one-day acquisition time interval). It is referred to as the three-pass approach if one SAR image is common to both interferometric pairs. In many cases, the use of a DEM turns out to be more robust and operationally practicable. The phase unwrapping required in the multi-pass approach is often difficult to resolve and far from operational for low coherence areas, especially in rugged terrain. In addition, gaps in the unwrapped topographic phase for areas of too low coherence may be present, depending on the phase unwrapping method used. Previous to subtraction from the complex interferogram, the topography-related phase term has to be scaled according to the perpendicular baseline component (Equation 4). The exact knowledge of the baseline is therefore very important. At present, we use various estimation methods based on the orbit data, the image-to-image registration offsets, and the fringe rate of the interferograms. For two-pass differential SAR interferometry, but also in order to combine the information retrieved by the SAR system with other information in map coordinates, geocoding (i.e., the transformation between the range-Doppler coordinates of the SAR and orthonormal map coordinates) is required. For automatic terrain corrected SAR geocoding with a DEM in orthonormal coordinates, we use the approach presented by Wegmüller (1999).

Once the differential interferogram is computed, the phase has to be unwrapped. From the interferogram, the interferometric phase is only known to Modulo 2π and the correct multiple of 2π has to be added. Phase unwrapping is a problematic step due to discontinuities and inconsistencies as a result of high phase noise. In a first step, filtering and multi-looking are used to reduce the phase noise (Goldstein and Werner, 1997). Then, phase unwrapping is done by applying a region-growing algorithm to the filtered interferogram (Rosen *et al.*, 1994). Critical areas with very low coherence and inconsistencies are identified and avoided in the phase unwrapping.

In a final step, the unwrapped phase is converted to a displacement value. A geocoded map of displacement values per pixel is the final product of differential SAR interferometry.

Interferogram Stacking Technique

Phase distortions caused by spatially heterogeneous atmospheric (in particular, water vapor) and ionospheric conditions limit the accuracy of differential SAR interferometry. Large atmospheric distortions can often be identified by their specific shape, by cross-comparison of interferograms, or possibly based on meteorological data. It is not clear, though, how to best integrate such tests in an operational processing chain.

The goal of our analysis is to achieve an operational and robust technique. For this reason, we take a conservative assumption on the atmospheric distortions in single interferograms. As a typical atmospheric distortion, we consider a relative high phase error of $\pi/2$, which corresponds for the ERS SAR configurations to an error of approximately 0.7 cm in the estimation of the displacement. In order to obtain reliable displacement estimates, the displacement signal should dominate over the error term. In order to keep the expected error on the order of 5 percent, the displacement phase term has to be 20 times the assumed atmospheric distortion, i.e., 10π or 5 fringes, corresponding to around 14 cm of displacement for the ERS SAR configurations. Because the displacement increases with increasing acquisition time interval, interferometric pairs with long acquisition time intervals are preferred to reduce the effect of the atmospheric distortions. For instance, we preferably select an interferogram with three or more years acquisition time interval to map the displacement of an area with velocities up to 5 cm/year. In order to map faster displacement velocities, shorter intervals are preferred to study the temporal dynamic of the displacement. For slower displacement velocities, even longer intervals would be required. The time interval cannot be extended much beyond a few years because of data availability and because the use of very long time intervals introduces excessive temporal decorrelation that precludes interpretation of the data. A welcome approach to improve the ratio between the displacement signal and the atmospheric phase errors is the stacking of interferograms. Under the assumption of a stationary process (i.e., assuming that the displacement velocity is constant in time), the displacement terms add up linearly, whereas the atmospheric errors (for which we can assume statistical independence for independent interferograms) increase only with the square root of the number of pairs considered.

The mathematical framework of the stacking technique is simple. Let us consider n independent interferograms with different acquisition time intervals t_j and unwrapped phase ϕ_j. The sum of all t_j results in a total acquisition time interval t_{cum} and the sum of all ϕ_j results in a cumulative unwrapped phase ϕ_{cum}. The average displacement velocity along the look direction v_{disp} is computed as

$$v_{disp} = \frac{\lambda \cdot \phi_{cum}}{4\pi \cdot t_{cum}} \quad (10)$$

and the displacement velocity estimation error as

$$\Delta v_{disp} = \frac{\lambda \cdot \sqrt{n} \cdot E}{4\pi \cdot t_{cum}}. \quad (11)$$

Here, E is the assumed phase error of a single interferograms (e.g., $\pi/2$) and λ is the wavelength. Equations 10 and 11 can be used to determine the cumulative time t_{cum} required to map a certain displacement velocity v_{disp} with a predefined expected relative estimation error. The potential of the stacking technique is demonstrated by the fact that the stacking of more than ten independent interferograms with atmospheric distortions up to $\pi/2$ allows a cumulative time interval of more than 20 years to be reached and results in an expected displacement velocity estimation error of around 1 mm/year. Such interferogram stacking is made possible by the immense ERS SAR data archive.

In a real case, not all interferograms may be statistically independent because a SAR image may be used for various pairs. In this case, the expected relative error is larger than the one computed with Equation 11. In addition, due to different ground conditions and spatial baselines, the coherence of the interferograms may be different, resulting in a different coverage with unwrapped-phase information. In our methodology, a displacement value is only determined for points with more than a certain number of valid values. Finally, because interferogram stacking is based on the assumption of stationary displacement velocities, information on the temporal dynamic of the displacement is lost.

Error Estimations for a Successful Application of the Technique

The successful application of differential SAR interferometry for surface displacement mapping depends on factors related to the phenomenon itself (displacement velocity field, temporal and spatial gradients), scene parameters (topography, land use), sensor parameters (data availability, acquisition time interval, baseline), the availability and accuracy of a DEM, and data processing related factors (baseline estimation, phase unwrapping, geocoding, stacking of interferograms).

The assumption of a known displacement direction is usually appropriate in the case of subsidence caused by ground water extraction where the displacement is nearly vertical. In the case of mining-induced ground movement, on the other hand, the deformation geometry is more complicated and even a combination of SAR data acquired in ascending and descending modes does not allow the resolution of the complete three-dimensional displacement field without the use of additional information.

Information on the displacement velocity field and, in particular, on its temporal and spatial gradients is, if available, very important for the selection of the most appropriate SAR data with respect to the acquisition time interval. In order to transform the displacement phase term to an absolute displacement velocity, a reference point is required. Often the scene content does permit the specification of stable points. In other cases, leveling surveys or GPS measurements may provide the reference point.

Scene topography and land use also have an influence on the accuracy and robustness of the interferometric technique. The estimation of the displacement phase term requires the prior estimation of the topographic phase term. Inaccuracies in the DEM directly translate into errors in the displacement measurement (see Equation 4). In addition, in areas of very rugged topography, the successful application of SAR data is strongly reduced by the particular imaging geometry of the sensor. The land use affects the coherence. For acquisition time intervals longer than one year, high coherence is mainly found in urban and suburban areas.

Sensor parameters such as the wavelength, the spatial resolution, and the incidence angle have a strong influence on the feasibility of the SAR interferometric displacement mapping. Such factors are not discussed here, because the examples shown are based only on SAR data from the ERS satellites. Data availability is another factor that affects the possibility of generating subsidence maps. While for most of the European sites a large number of ERS acquisitions are available, allowing the optimization of the data selection with respect to acquisition dates and interferometric baselines, for some regions in developing countries only a small amount of ERS SAR data was acquired.

Data processing related aspects, which influence the robustness and operationality of the application, include baseline estimation, phase unwrapping, geocoding, and the stacking of interferograms. Not so much the optimization of the processing for a specific example, but a robust processing scheme that works under most circumstances is the major objective. In our processing chain, we identified phase unwrapping and baseline estimation as the most critical points. The geocoding scheme, on the other hand, turns out to be operational and robust when an external DEM is used (Wegmüller, 1999).

Phase unwrapping is a difficult task because the coherence in long time-delay interferograms tends to be very low for large parts of the image. In some cases, patches of coherence sufficiently high to reliably interpret the interferometric phase are disconnected in space and separated by areas with high phase noise. The unwrapping of sparse data may be successfully achieved if accurate subsidence models are available or if the subsidence geometry is simple and the displacement rate slow (Costantini and Rosen, 1999).

Errors in the estimation of the baseline affect the scaling of the topography-related phase and the flattening of the interferogram (i.e., the removal of the fringe frequency corresponding to a flat surface) in range and azimuth directions. We first consider the relationship between a change in the topographic height ∂z and the corresponding change in the interferometric phase $\partial\phi$ (Equation 4). An error $\delta B_\perp$ in the estimation of the perpendicular baseline affects the scaling of the topographic height, resulting in a phase difference error $\delta(\partial\phi)$. By transforming $\delta(\partial\phi)$ to a displacement error $\delta(r_{disp})$, Equation 5 for the ERS configuration can be rewritten as

$$\delta(r_{disp}) = 3.0 \cdot 10^{-6} \partial z \delta B_\perp [m]. \quad (12)$$

A typical estimation error of the perpendicular baseline of 0.1 m for a height change of 100 m results in a displacement error of 0.03 mm. For relatively flat terrain, the scaling of the interferogram is therefore not a significant problem.

Further, we consider baseline estimation errors affecting the flattening of the interferogram in the slant-range direction y (Equation 6). An error $\delta B_\perp$ in the estimation of the perpendicular baseline results in an error $\delta(\partial\phi)$ in the phase difference in the range direction. In the case of the ERS configuration, this corresponds to a displacement error $\delta(r_{disp})$ of

$$\delta(r_{disp}) = 2.8 \cdot 10^{-6} \partial y \delta B_\perp [m]. \quad (13)$$

A typical estimation error for the perpendicular baseline of 0.1 m results in a displacement error of 2.8 mm in a 10-km distance. Therefore, flattening is a critical step in subsidence measurements of large areas, and the required baseline-estimation accuracy is high. Stacking of interferograms may reduce the errors caused by flattening because the baseline estimation error can be assumed to be statistically independent for the different interferograms.

Finally, we consider baseline estimation errors affecting the flattening of the interferogram in the azimuth direction x (Equation 7). An error $\delta(\partial B_\parallel/\partial x)$ in the estimation of the change of $B_\parallel$ along the line of flight results in an error $\delta(\partial\phi)$ in the phase

TABLE 1. ESTIMATED SUBSIDENCE VELOCITIES FOR THE SELECTED SITES. IN ALL CASES ERS SAR DATA ARE USED. THE EXPECTED ACCURACY IS COMPUTED ASSUMING AN ATMOSPHERIC DISTORTION OF $\pi/2$. NO OTHER ERRORS ARE CONSIDERED

Site	Velocities [cm/year]	Monitoring interval	Number of interferograms	Cumulative time interval	Expected accuracy [cm/year]
Ruhrgebiet (Germany)	0–200	1 month	1	1 month	9.0
Mexico City (Mexico)	0–40	3 months	2	6 months	2.0
Bologna (Italy)	0–6	1 year	6	4 years	0.5
Euganean Geothermal Basin (Italy)	0–0.4	5 years	10	20 years	0.1

difference in the azimuth direction. Transforming the phase-difference error into a displacement error $\delta(r_{disp})$ results, for the ERS configuration, in

$$\delta(r_{disp}) = \partial y \delta(\partial B_{\parallel}/\partial x)\ [m]. \quad (14)$$

A typical estimation error for the parallel baseline change of 5 cm per 100 km results in a displacement error of 5 mm for a 10-km distance in azimuth. The flattening of the interferogram in the azimuth direction is again a critical step for the monitoring of large areas.

Results of Land Subsidence Maps

The ERS satellites carry SAR instruments suitable for interferometric data analysis. Their 35-day repeat-orbit cycle is appropriate for subsidence monitoring in most of the cases. The large archive of ERS SAR data available since 1991 allows subsidence studies with SAR interferometry in many regions around the world. For this analysis, we selected four sites characterized by different land use, topography, and temporal and spatial dependence of the movement (see Table 1): the Ruhrgebiet (Germany), Mexico City (Mexico), the Euganean Geothermal Basin (Italy), and Bologna (Italy). While a single successful example is sufficient to demonstrate the potential of a technique, the analysis of several cases allows us to assess its maturity and operational readiness. A more detailed description of these studies can be found in Wegmüller *et al.* (2000), Strozzi and Wegmüller (1999), Strozzi *et al.* (1999), and Strozzi *et al.* (2000b).

In all cases, SAR processing was performed to the same Doppler centroid in order to maximize the fringe visibility (Werner *et al.*, 2000). All the complex SAR images were then registered with sub-pixel accuracy to the same reference geometry. The interferograms were calculated with five looks in azimuth and one look in range (ten looks in azimuth and two looks in range for Mexico City) using spectral shift filtering. Based on the orbit parameters and the average interferogram fringe frequency, the baseline was estimated. For the two Italian

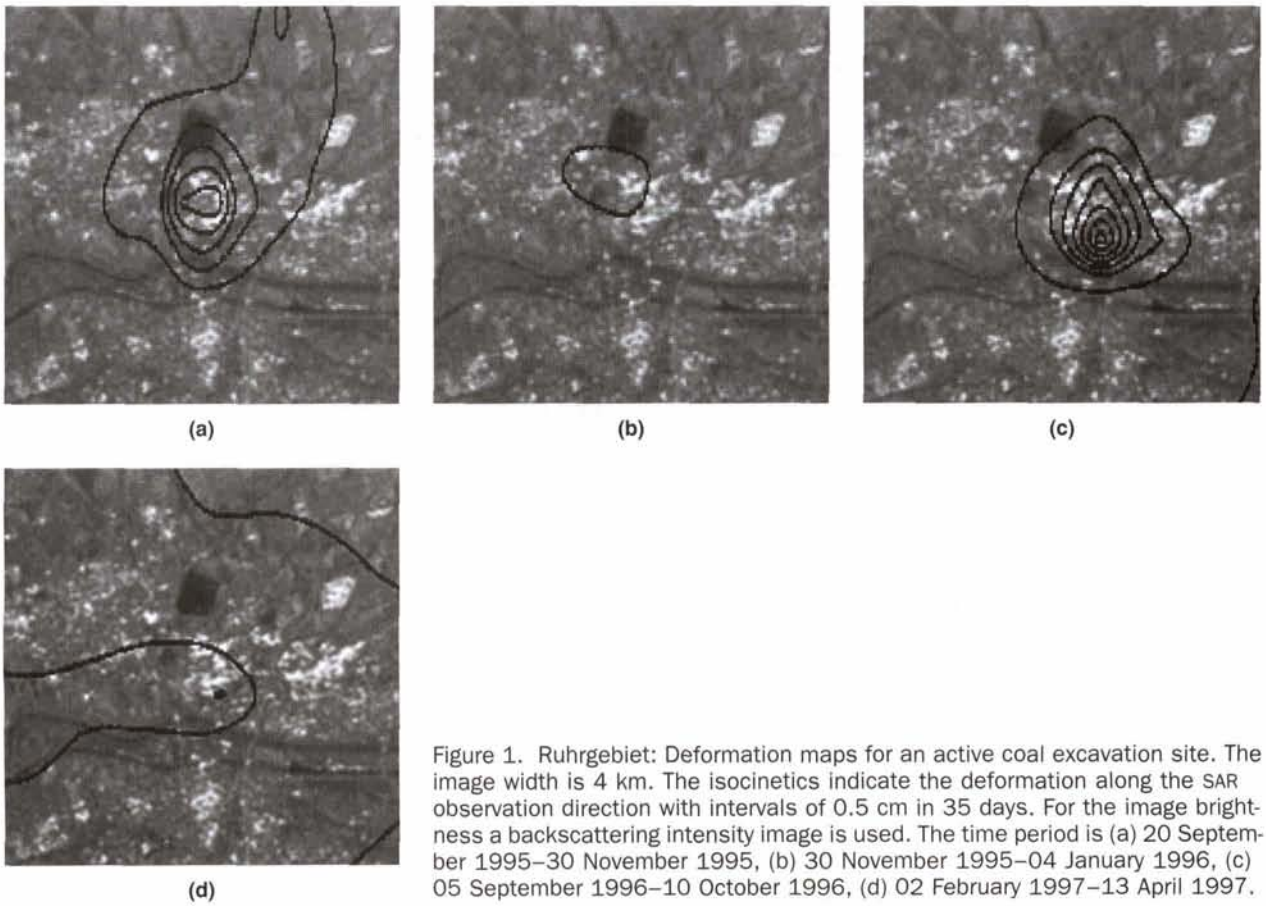

Figure 1. Ruhrgebiet: Deformation maps for an active coal excavation site. The image width is 4 km. The isocinetics indicate the deformation along the SAR observation direction with intervals of 0.5 cm in 35 days. For the image brightness a backscattering intensity image is used. The time period is (a) 20 September 1995–30 November 1995, (b) 30 November 1995–04 January 1996, (c) 05 September 1996–10 October 1996, (d) 02 February 1997–13 April 1997.

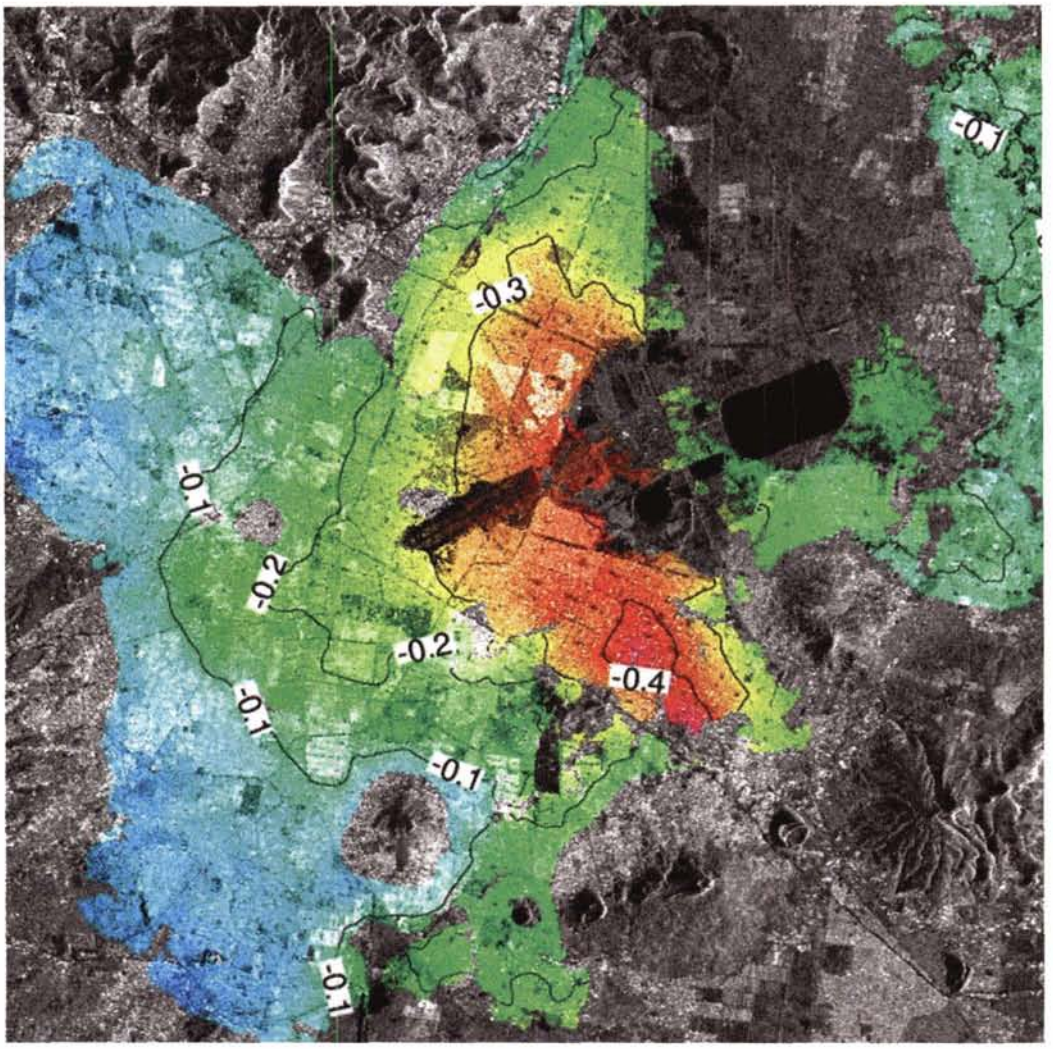

Plate 1. Mexico City: SAR interferometric subsidence map (in m/year) derived from two ERS pairs between December 1995 and May 1996. The backscattering coefficient is used as image brightness. The image width is about 30 km.

sites, a precision DEM was used to subtract the topographic phase; in the other two cases, an ERS-1/2 Tandem pair was employed. The phase was unwrapped after filtering but only for areas of sufficiently high coherence. The interferogram stacking technique was used with the SAR data of Bologna and of the Euganean Geothermal Basin where the subsidence rates are low and nearly uniform in time. In a final step, terrain corrected geocoding to a pixel size of 25 m (50 m for Mexico City) was performed. For the validation of the subsidence maps with leveling data, a geocoding refinement step using ground-control points extracted from topographic maps was necessary.

Ruhrgebiet

Coal mining in the German Ruhrgebiet causes significant surface movement (Drecker *et al.*, 1995; Fischer and Spreckels, 1999). Because of legal requirements, the mining companies are obliged to assess the environmental impact of the excavations. Surface movement caused by mining is a very dynamic process with high spatial and temporal variability. For mining areas with high subsidence velocities, interferometric pairs with acquisition time intervals of only one or a few 35-day repeat cycles are most appropriate. Subsidence maps of different time intervals, as shown in Figures 1a to 1d, clearly indicate the progress in the sub-surface coal excavation. The displacement was computed in the look direction of the satellites because the vertical direction of the mining-induced subsidence cannot be assumed. The maximum displacement in 35 days was on the order of 4 cm.

Mexico City

Mexico City is built on highly compressible clays and, by reason of strong groundwater extraction, a total subsidence of more than nine meters has been observed over the last century (Figueroa Vega, 1976; Rivera, 1990). The selection of ERS data to map subsidence is Mexico City is strongly restricted by the relatively few acquisitions found in the archive. From the available data acquisitions, two independent differential interferograms in ascending and descending modes, both with an acquisition time interval of 139 days, were selected (Strozzi and Wegmüller, 1990). Consistent results were found with the two interferograms, and their results were averaged. For the time period December 1995 to May 1996 (Plate 1), the observed maximum subsidence velocity was larger than 40 cm/year, in agreement with the results of leveling surveys and theoretical models.

Bologna

At Bologna, Italy, land subsidence is caused by ground-water exploitation for industrial, domestic, and agricultural uses (Barbarella *et al.*, 1990; Balestra and Villani, 1991; Capra *et al.*, 1991; Bitelli *et al.*, 2000). Maximum subsidence velocities of 6 to 8 cm/year were observed with precision leveling surveys during the time period 1987–1991. We produced two subsidence maps for the time periods 1992–1993 (Figure 2a) and 1997–1998 (Figure 2b) using in both cases six ERS SAR data and the interferogram stacking technique (Strozzi *et al.*, 2000b). The comparison of the two subsidence maps shows a decrease in the subsidence velocity from 1992–1993 to 1997–1998. The leveling surveys performed in 1987 and 1991 were used for validation of the subsidence map derived from ERS differential SAR interferometry between 1992 and 1993. The time difference between leveling and SAR data was not considered significant for the validation because between 1983 and 1991 land subsidence in Bologna has been relatively constant (Folloni *et al.*, 1996). For 215 points distributed over the urban area of Bologna, the average difference between the SAR interferometric subsidence results of the time period 1992–1993 and the leveling data of 1987 and 1991 is 0.4 cm/year with a standard deviation of 0.9 cm/year. The minimum and maximum differences are −3.7 and +2.6 cm/year, respectively. The small standard deviation of 0.9 cm/year between the data from the two methods indicates a good performance of ERS differential SAR interferometry for subsidence mapping in urban areas. The systematic offset between the two data sets can be explained by the different time period, indicating a decrease in the subsidence velocity. This conclusion is confirmed by a more detailed comparison performed along the three leveling lines shown in Figure 3. The profiles of Figure 4 indicate similar behaviors of the two data sets, with smaller subsidence velocities for the SAR data.

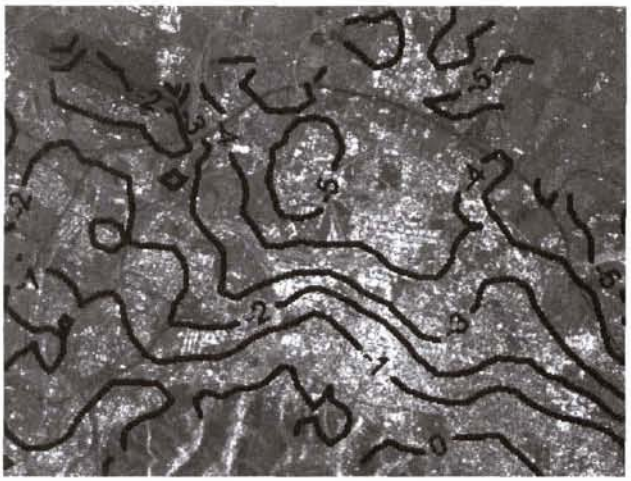

(a)

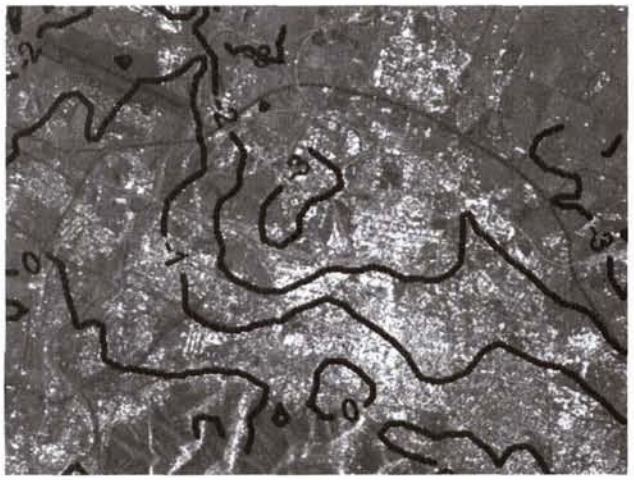

(b)

Figure 2. SAR interferometric subsidence maps (in cm/year) in Bologna for the time periods 1992–1993 (a) and 1997–1998 (b). The backscattering coefficient is used as image brightness.

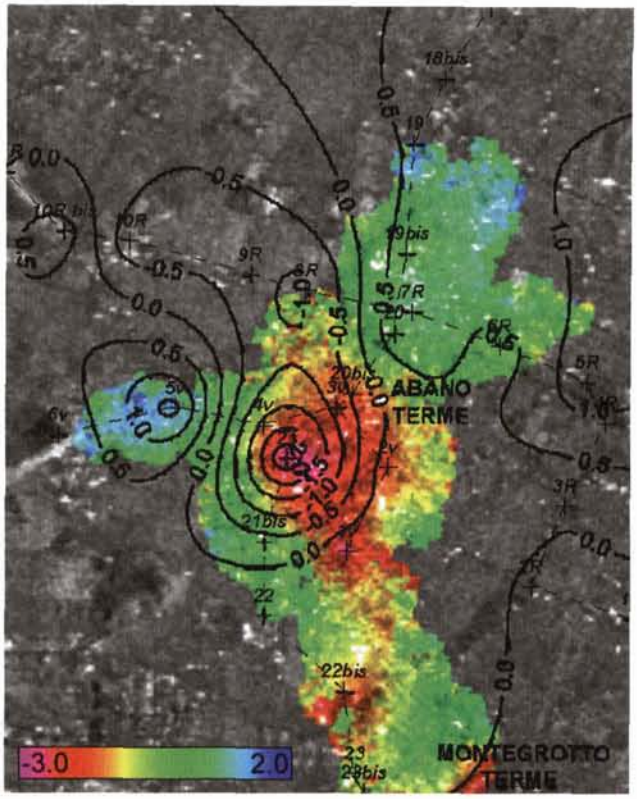

Plate 2. Map of the vertical ground movements (in mm/year) from two leveling surveys in 1991 and 1995 in the urban areas of Abano and Montegrotto Terme (data from Comune di Abano Terme and Regione del Veneto) superimposed on the ERS interferometric displacement velocity map for the time interval 1992 and 1996 (in mm/year). Also shown is the position of the benchmarks (+). The image width is about 4.5 km.

Euganean Geothermal Basin

Land subsidence in the Euganean Geothermal Basin, Italy, is related to the geothermal groundwater withdrawal (Brighenti, 1991; Gottardi, 1995). Up to 1991 the maximum rate of land subsidence has been 1 cm/year as observed from precision leveling surveys. After 1991 the subsidence velocity decreased as a consequence of the regulation of groundwater exploitation. In order to map the expected low sub-cm/year displacement velocity, ten ERS SAR interferograms in the time span 1992 to 1996 were selected (Strozzi *et al.*, 1999). Interferogram stacking was applied to generate a single map with a cumulative time interval of more than 20 years. The resulting interferometric map shown in Plate 2 reveals a clear subsidence signal over

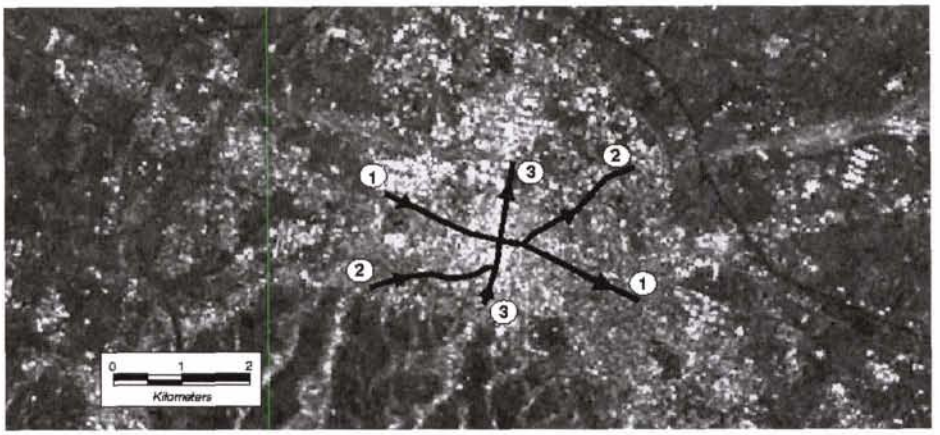

Figure 3. Leveling lines selected for the comparison of the subsidence velocities derived from ERS SAR interferometry and leveling surveys.

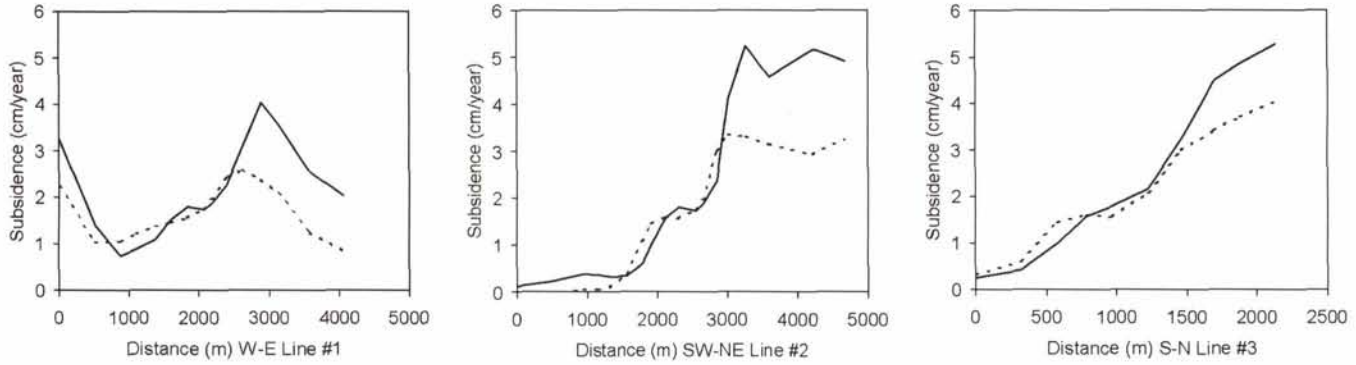

Figure 4. Profiles of the subsidence velocities determined from ERS SAR interferometry (period 1992–1993, dotted lines) and leveling surveys (period 1987–1992, normal lines) along the three leveling lines shown in Figure 3.

Abano Terme with a maximum vertical displacement velocity of 3 mm/year, in agreement with the results of the last leveling surveys performed in 1991 and 1995. The high correspondence of the results of the two different surveying techniques is confirmed by a direct quantitative comparison along the leveling lines, an example of which is shown in Figure 5. For the 17 points where we have values available from both SAR interferometry and leveling, the average difference of the vertical displacement velocity values is 0.2 mm/year with a standard deviation of 1.0 mm/year. The minimum and maximum differences are −1.5 mm/year and +2.2 mm/year, respectively. This result confirms the expected high accuracy that can be achieved with the interferogram stacking technique.

Conclusions

The high potential of differential SAR interferometry to monitor a wide range of deformation velocities ranging from m/year to mm/year was demonstrated by the generation of subsidence maps for the Ruhrgebiet, Mexico City, Bologna, and the Euganean Geothermal Basin. With our understanding of the influence of several important factors related to the subsidence phenomenon, the sensor, the scene, and the data processing, we are now in the position for new subsidence cases to evaluate the strategy to use, to assess the expected processing effort, and

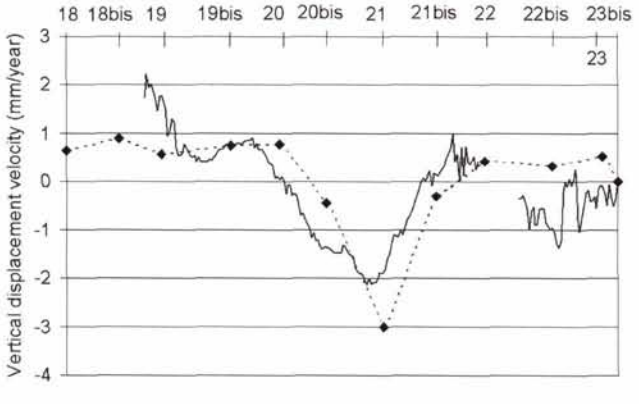

Figure 5. Profiles of the vertical displacement velocity from ERS SAR interferometry (continuous line, period 1992–96) and leveling surveys (dotted line, period 1991–95, data from Comune di Abano Terme and Regione del Veneto) along the leveling line Abano Terme—Montegrotto Terme.

to indicate the accuracy. In spite of this operational readiness, it is important to keep in mind the limitations of the technique. In most cases, it was not possible, for example, to generate a subsidence map with complete coverage due to temporal decorrelation for certain land-cover types.

The service provided by differential SAR interferometry is not intended to replace such conventional techniques as leveling surveys and GPS measurements. On the contrary, the comparison of the characteristics of SAR interferometry, leveling surveys, and GPS measurements indicates advantages and disadvantages of these techniques, individually used, that should be considered for an accurate, rational, and cost-effective monitoring of subsidence. SAR interferometry gives a two-dimensional spatial coverage over urban areas but does not work over vegetated zones. In addition, because ERS SAR data are regularly acquired every 35 days, information can always be retrieved without the need for planning new measurements. Other advantages of differential SAR interferometry are the cost, which is many times lower than that of leveling surveys (offering the opportunity to regularly repeat the measurements), and its application in near real time. Leveling surveys, on the other hand, are restricted to lines but can be used with high precision over all land use classes. Furthermore, benchmarks can be precisely fixed over buildings exposed to damage. Finally, GPS measurements can support differential SAR interferometry in the identification of a reference point and for the monitoring of very large areas.

The availability of ERS SAR data contributes to the usefulness of this remote-sensing application. A further stimulus to the use of differential SAR interferometry for Earth surface displacement studies will be provided by the launch of ESA's ENVISAT spacecraft carrying an Advanced SAR and of NASDA's ALOS spacecraft with the PALSAR. Keeping in mind that the valuable archive of ERS SAR data useful for the displacement application is the result of the operation of the ERS satellites in the single mode (35-day repeat orbits) for most of the time it is essential that the SAR's of the ENVISAT and ALOS missions be operated in a single interferometric mode for most of the time.

Acknowledgments

This work was supported by an ESA Data User Program (DUP). The Italian National Geologic Survey is acknowledged for the DEM of the Italian sites. Arch. Benetetto Vettore of the Comune di Abano Terme and Ing. Andrea Costantini of the Regione del Veneto are acknowledged for the high precision leveling data of the Euganean Geothermal Basin. ERS SAR data acquired over Mexico City were courtesy of AO3-178.

References

Balestra, M., and B. Villani, 1991. Study of the subsidence in the Bolognese Area, *Proceedings of the Fourth International Symposium on Land Subsidence*, 12–17 May, Houston, Texas (IAHS Publ. No. 200), pp. 71–80.

Bamler, R., and P. Hartl, 1998. Synthetic aperture radar interferometry, *Inverse Problems*, 14:R1–R54.

Barbarella, M., L. Pieri, and P. Russo, 1990. Studio dell'abbassamento del suolo nel territorio bolognese mediante livallazioni ripetute: analisi dei movimenti e considerazioni statistiche, *INARCOS*, 506:1–19.

Barends, F., F. Brouwer, and F. Schröder, 1995. *Land Subsidence*, Balkema, Rotterdam, The Netherlands (ISBN 90 5410 589 5), pp. XI–XIV.

Bertoni, W., G. Brighenti, G. Gambolati, G. Ricceri, and F. Vuillermin, 1995. Land subsidence due to gas production in the on- and offshore natural gas fields of the Ravenna area, Italy, *Proceedings of the Fifth International Symposium on Land Subsidence*, 16–20 October, The Hague, The Netherlands (IAHS Publ. No. 234), pp. 13–20.

Bitelli, G., F. Bonsignore, and M. Unguendoli, 2000. Levelling and GPS networks for ground subsidence monitoring in the southern Po Valley, *Journal of Geodynamics*, 30(3):355–369.

Brighenti, G., 1991. Land subsidence due to thermal water withdrawal: The case of Abano Terme, northern Italy, *Proceedings of the Fourth International Symposium on Land Subsidence*, 12–17 May, Houston, Texas (IAHS Publ. No. 200), pp. 515–523.

Capra, A., G. Folloni, and P. Russo, 1991. Subsidence controls in the town of Bologna, *Proceedings of the Fourth International Symposium on Land Subsidence*, 12–17 May, Houston, Texas (IAHS Publ. No. 200), pp. 443–452.

Carbognin, L., L. Tosi, and P. Teatini, 1995. Analysis of actual land subsidence in Venice and its hinterland (Italy), *Land Subsidence* (F. Barends, F. Brouwer, and F. Schröder, editors), Balkema, Rotterdam, The Netherlands (ISBN 90 5410 589 5), pp. 129–137.

Costantini, M., and P. Rosen, 1999. A generalized phase unwrapping approach for sparse data, *Proceedings of IGARSS'99*, 28 June–02 July, Hamburg, Germany, (on CD ROM).

Drecker, P., D. Genske, K. Heinrich, and H. Noll, 1995. Subsidence and wetland development in the Ruhr district of Germany, *Proceedings of the Fifth International Symposium on Land Subsidence*, 16–20 October, The Hague, (IAHS Publ. No. 234), pp. 413–421.

Ferretti, A., C. Prati, and F. Rocca, 1999. Monitoring terrain deformation using multi-temporal SAR images, *Proceedings of the CEOS SAR Workshop*, 26–29 October, Toulouse, France, (on CD ROM).

Figueroa Vega, G., 1976. Subsidence of the City of Mexico; a historical review, *Proceedings of the Anaheim Symposium*, December, Anaheim, California (IAHS Publication No. 121), pp. 35–38.

Fischer, C., and V. Spreckels, 1999. Environmental Monitoring of coal mining subsidences by Airborne High Resolution Scanner, *Proceedings of IGARSS'99*, 28 June–02 July, Hamburg, Germany, (on CD ROM).

Folloni, G., P. Russo, and F. Radicioni, 1996. La subsidenza del territorio bolognese dal 1983 al 1993, *INARCOS*, 571:400–413.

Fruneau, B., J.P. Rudant, D. Obert, and D. Raymond, 1999. Small displacements detected by SAR interferometry on the City of Paris (France), *Proceedings of IGARSS'99*, 28 June–02 July, Hamburg, Germany, (on CD ROM).

Gatelli, F., A. Monti Guarnieri, F. Parizzi, P. Pasquali, C. Prati, and F. Rocca, 1994. The wavenumber shift in SAR interferometry, *IEEE Trans. Geosci. Remote Sensing*, 32(4):855–865.

Goldstein, R., R. Engelhardt, B. Kamb, and R. Frolich, 1993. Satellite radar interferometry for monitoring ice sheet motion: Application to an Antarctic ice stream, *Science*, 262:1525–1530.

Goldstein, R., and C. Werner, 1997. Radar ice motion interferometry, *Proceedings of the Third ERS Symposium*, 17–21 March, Florence, Italy, pp. 969–972.

Gottardi, G., P. Previatello, and P. Simonini, 1995. An extensive investigation of land subsidence in the Euganean Geothermal Basin, Italy, *Proceedings of the Fifth International Symposium on Land Subsidence*, 16–20 October, The Hague, The Netherlands (IAHS Publ. No. 234), pp. 21–30.

Joughin, I., R. Kwok, and M. Fahnestock, 1996. Estimation of ice-sheet motion using satellite radar interferometry: Method and error analysis with application to Humboldt Glacier, Greenland, *Journal of Glaciology*, 42(142):564–575.

Massonet, D., M. Rossi, C. Carmona, F. Adragna, G. Peltzer, K. Feigl, and T. Rabaute, 1993. The displacement field of the Landers earthquake mapped by SAR interferometry, *Nature*, 364:138–142.

Massonet, D., P. Briole, and A. Arnaud, 1995. Deflation of the Mount Etna monitored by spaceborne radar interferometry, *Nature*, 375:567–570.

Mohr, J.J., N. Reeh, and S.N. Madsen, 1998. Three-dimensional glacial flow and surface elevation measured with radar interferometry, *Nature*, 391:273–276.

Mohr, J.J., and S.N. Madsen, 1999. Error analysis for interferometric SAR measurements of ice sheet flow, *Proceedings of IGARSS'99*, 28 June–02 July, Hamburg, Germany, (on CD ROM).

Poland, J.F., 1984. *Guidebook to Studies of Land Subsidence Due to Ground-Water Withdrawal, prepared for the International Hydrological Programme, Working Group 8.4, UNESCO, Book Crafters, Chelsea, Massachusetts, 16 p.*

Rivera, A., 1990. *Modèle hydrogéologique quasi-tridimensionnel non-linéaire pour simuler la subsidence dans les systèmes aquifères multicouches. Cas de Mexico*, Ph.D. Thesis, Ecole National Supérieure des Mines de Paris, CIG Paris, France.

Rodriguez, E., and J. Martin, 1992. Theory and design of interferometric Synthetic-Aperture Radars, *IEE Proceedings F*, 139(2):147–159.

Rosen, P., C. Werner, and A. Hiramatsu, 1994. Two-dimensional phase unwrapping of SAR interferograms by charge connection through neutral trees, *Proceedings of IGARSS'94*, 08–12 August, Pasadena, California.

Strozzi, T., and U. Wegmüller, 1999. Land subsidence in Mexico City mapped by ERS differential SAR interferometry, *Proceedings of IGARSS'99*, 28 June–02 July, Hamburg, Germany, (on CD ROM).

Strozzi, T., L. Tosi, L. Carbognin, U. Wegmüller, and A. Galgaro, 1999. Monitoring land subsidence in the Euganean Geothermal Basin with differential SAR interferometry, *Proceedings of FRINGE'99*, 10–12 November, Liege, Belgium, (on CD ROM).

Strozzi, T., P. Dammert, U. Wegmüller, J.M. Martinez, J. Askne, A. Beaudoin, and M. Hallikainen, 2000a. Landuse mapping with ERS SAR interferometry, *IEEE Trans. Geosci. Remote Sensing*, 38(2):766–775.

Strozzi, T., G. Bitelli, and U. Wegmüller, 2000b. Differential SAR interferometry for land subsidence mapping in Bologna, *Proceedings of SISOLS 2000*, 25–29 September, Ravenna, Italy, 2:187–192.

Wegmüller, U., 1999. Automated terrain corrected SAR geocoding, *Proceedings of IGARSS'99*, 28 June–02 July, Hamburg, Germany, (on CD ROM).

Wegmüller, U., T. Strozzi, and C. Werner, 1998. Characterization of differential interferometry approaches, *Proceedings of EUSAR'98*, 25–27 May, Friedrichshafen, Germany.

Wegmüller, U., T. Strozzi, C. Werner, A. Wiesmann, N. Benecke, and V. Spreckels, 2000. Monitoring of mining-induced surface deformation in the Ruhrgebiet (Germany) with SAR interferometry, *Proceedings of IGARSS 2000*, 24–28 July, Honolulu, Hawaii, (on CD ROM).

Werner, C., U. Wegmüller, T. Strozzi, and A. Wiesmann, 2000. Gamma SAR and interferometric processing software, *Proceedings of ERS-ENVISAT Symposium*, 16–20 October, Gothenburg, Sweden, (on CD ROM).

Zebker, H., T. Farr, R. Salazar, and T. Dixon, 1994. Mapping the World's topography using radar interferometry: The TOPSAT mission, *Proceedings of the IEEE*, 82(12):1774–1786.

(Received 17 June 2000; accepted 12 February 2001; revised 21 March 2001)